Paleontological Research

Papers in Press

"Papers in Press" includes peer-reviewed, accepted manuscripts of research articles, reviews, and short notes to be published in Paleontological Research. They have not yet been copy edited and/or formatted in the publication style of *Paleontological Research*. As soon as they are printed, they will be removed from this website. Please note they can be cited using the year of online publication and the DOI, as follows:

Humblet, M. and Iryu, Y. 2014: Pleistocene coral assemblages on Irabu-jima, South Ryukyu Islands, Japan. *Paleontological Research*, doi: 10.2517/2014PR020.

doi:10.2517/2019PR020

A morphological analysis of the flat-shaped spumellarian radiolarian *Dictyocoryne*: morpho-functional insights into planktonic mode of life

YUTA SHIINO[1], TOSHIYUKI KURIHARA[2], RYO ICHINOHE[3], NAOKO KISHIMOTO[4], TAKASHI YOSHINO[5] AND ATSUSHI MATSUOKA[6]

[1] *Department of Geology, Niigata University, 8050, Ikarashi 2-no-cho, Nishi-ku, Niigata 950-2181, Japan (email: y-shiino@geo.sc.niigata-u.ac.jp)*

[2] *Graduate School of Science and Technology, Niigata University, 8050, Ikarashi 2-no-cho, Nishi-ku, Niigata 950-2181, Japan*

[3] *Atmosphere and Ocean Research Institute, The University of Tokyo, 5-1-5, Kashiwanoha, Kashiwa-shi, Chiba 277-8564, Japan*

[4] *Department of Mechanical Engineering, Setsunan University, 17-8, Ikeda-Nakamachi, Neyagawa, Osaka 572-8508, Japan*

[5] *Department of Mechanical Engineering, Toyo University, Kujirai 2100, Kawagoe, Saitama 350-8585, Japan*

[6] *Department of Geology, Niigata University, 8050, Ikarashi 2-no-cho, Nishi-ku, Niigata 950-2181, Japan*

Abstract. The three-dimensional morphology of the flat-shaped spumellarian radiolarian *Dictyocoryne* was analysed using a microfocus X-ray CT with a special focus on whether it was capable of a planktonic lifestyle. Two types of 3D models, the shell model, which represents realistic 3D shell, and the wrapped model, which mimics the whole body outline without axopodia, were reconstructed in order to estimate volume,

surface area, and centre of gravity for the shell model and buoyancy for the wrapped model. The calculated values showed that the volume of shell with respect to the total volume was negatively allometric, regardless of the differences between threshold settings. Stepwise secretions of the patagium layer may result in a comparatively lightweight shell, thereby decreasing the total density during growth but not below the density of seawater. Estimated positions for the centres of gravity and buoyancy were too close to maintain an autonomous posture while floating. Instead, the ratio between surface area and volume was greater than that in an ideal sphere. Such a broad surface area could obtain the viscous resistance necessary for sinking retardation. Spumellarian radiolarians, including *Dictyocoryne*, have photosynthetic symbionts located primarily in the ectoplasmic layer, which is a habitable space that can be maximised within the larger surface area. Given that radiolarians float when extending their pseudopodia, it can be hypothesised that pseudopodia may play a role in the adjustment of life posture in a hydraulically unstable shell, which can be integrated into sinking retardation, enhancement of photosynthetic activity and manoeuvrability of life posture within a unique flat-shaped morphogenesis.

Key words: computed tomography, ecomorphology, functionality, holoplankton, morphotype, scaling

Introduction

Techniques for biological imaging have revealed unknown and invisible structures regardless of the size and quality of the materials studied, and have provided basic evidence

for understanding morphological adaptation and evolution (e.g. Kaji *et al.*, 2011; Sutton *et al.*, 2014; Nomaki *et al.*, 2015, 2018; Shiino and Tokuda, 2016; Fujiwara, 2018). Microfocus X-ray CT is an innovative technology used for non-destructive morphological analyses via 3D modelling (Sutton *et al.*, 2014). 3D morphological data have resulted in new discoveries about internal features and their relationships with external morphology in both living and fossil organisms and within a wide range of body sizes. In the case of radiolarians, previous studies have been successful in 3D model reconstruction for emending taxonomic descriptions and reconsiderations (Matsuoka *et al.*, 2012; Ishida *et al.*, 2015; Yoshino *et al.*, 2015). Because radiolarians are of great biostratigraphic use, ranging from Cambrian to modern times, a functional morphological approach for 3D morphological data is necessary to reveal new principles of long-term evolution over geological time, as discussed to some extent in metazoan studies (e.g. Bramble and Lieberman, 2004; Rayfield, 2007; Shiino and Kuwazuru, 2010; Shiino *et al.*, 2014; Liu *et al.*, 2015).

The flat form of radiolarians represents one of the key morphological innovations that may have led to a new level of ecological performance within a planktonic mode of life. Among the living flat-shaped spumellarians, the genus *Dictyocoryne* is characterised by a triangular flat-shaped shell with a spongy structure, three arms and patagium (Matsuoka, 1992; Sugiyama and Anderson, 1997). In addition, one surface of the patagial shell close to the triple junction of the arms has a tubular passway (pylome) or a depression for a long, thick axopodium, the so-called axoflagellum (Matsuoka, 1992, 1994). The position and shape of the pylome or depression differ among species (Matsuoka, 1994). Because the axoflagellum is thought to function in buoyancy and posture control (Suzuki and Not, 2015; Ichinohe *et al.*, 2019), obverse and reverse faces might exist on the flat-shaped shell within its lifetime. However, the morphological differences between the two faces have never been analysed except for the characteristic pylome of the axoflagellum.

Apart from shell morphology, *Dictyocoryne* has many symbionts within the cell (e.g. Anderson, 1976, 1983; Takahashi *et al*., 2003; Yuasa *et al*., 2012; Zhang *et al*., 2018). The intensity of sunlight penetration decreases rapidly with seawater depth, and the optical conditions at approximately a 20 to 40 m depth, which is likely the main habitat for *Dictyocoryne* (Ishitani and Takahashi, 2007), are characterised by only a small amount of downwelling background light (e.g. Gordon and McCluney, 1975; Kirk, 1989). To avoid problems with photosynthetic activity, *Dictyocoryne* may require an appropriate posture within an equatorial plane, with the flat-shaped shell facing in an upward direction, similar to a solar panel.

The floating posture of *Dictyocoryne* has been discussed in previous studies based on the observation of culture experiments (Matsuoka, 1994; Ichinohe *et al*., 2019). Matsuoka (1994) reported that living *Dictyocoryne truncata* (Ehrenberg) frequently show a horizontal posture with the axoflagellum orienting downward. In contrast to the conclusion of Matsuoka (1994), Ichinohe *et al*. (2019) visualised a horizontal posture of *Dictyocoryne* with the axoflagellum extended upward. The mechanism responsible for this posture was explained in terms of the hydrodynamic function of the axoflagellum, where the ambient flow (even if an only few μm/s) rotates the axoflagellum toward the downstream direction, representing a so called weathercock effect (Ichinohe *et al*., 2019). Given that photosynthetic performance may experience dysfunction unless *Dictyocoryne* manages to sustain postural stability, it is hypothesised that the assumed differences between the obverse and reverse faces of the flat shell assisted in a homeostatic life posture, but there have been no precise examinations of the 3D morphology of these organisms.

The aim of this study was to produce a 3D model of *Dictyocoryne* using sequential images obtained via microfocus X-ray CT. Based on the morphological data, we examined the morphological characteristics of the siliceous shell and supposed living cell body of

Dictyocoryne, specifically addressing feasible life postures in the water column.

Material and methods

Using specimens of *Dictyocoryne*, 3D morphological data were constructed from X-ray CT images. The image-processing functions of a software package were used to estimate the volumes of the shell and the supposed cell without axopodia. The details of the applied methodology using microfocus X-ray CT have been described in previous reports (Matsuoka *et al*., 2012; Ishida *et al*., 2015).

Radiolarian specimens

Living radiolarians were collected as a reference offshore of Sesoko Island, Okinawa, Japan on 1st December 2008 and 27th November 2015 (Figure 1) on the research vessel "Euphoria 3" of the University of the Ryukyus (Ichinohe *et al*., 2018). At each locality, a plankton net (44 μm mesh) was used to sieve plankton, including radiolarians, at a 5 m depth. Using a Pasteur pipette, individuals of *Dictyocoryne* were separated from other planktonic organisms. All individuals were treated with a solution of H_2SO_4 to remove soft parts. Among the remaining shells, we subjected four skeletal specimens of *Dictyocoryne* to the microfocus X-ray CT. Based on shell morphology referred to Matsuoka (1993, 2009), we identified individuals as *Dictyocoryne profunda* Ehrenberg. This species is known to exhibit cyanobacterial symbionts in the extracytoplasm (Yuasa *et al*., 2012). Because there is no definition of body direction in the flat-shaped radiolarians, we refer to it in this study as shown in Figure 2, including key terminology following previous studies (Ogane and Suzuki, 2006; Suzuki and Aita, 2011) (Figure 2). The two faces of the flat shell of *Dictyocoryne profunda* Ehrenberg are distinguished by the presence of a pylome (or a depression) or its

absence (Matsuoka, 1992, 1994), representing the obverse or reverse face, respectively. The length of the individual is defined as the distance between the anterior end of the arm and the opposite side of the shell margin (Figure 2B), which is concordant with the height described by Matsuoka (1992).

Computed tomography

Sequential cross-sectional images of the specimens of *Dictyocoryne profunda* Ehrenberg were taken using Micro-CT in SEM (SkyScan, Belgium) (Figure 3). Subsequently, the volume data were translated into shell surface morphological data via the image-processing function of the structural analysis software VOXELCON 2014 (Quint Corporation, Japan). This data was referred to as “shell model” (Figure 3). Surface morphological data were subjected to the mesh-processing function of the computational fluid dynamics simulation software SC/Tetra (Cradle co. ltd., Japan), and smoothly wrapped volume data were generated as “wrapped model” herein. Each mesh for the wrapping was triangular in shape and 5 to 15 μm in size (Figure 3: wrapped model). Given that the volume of 3D data changes drastically with the differences in threshold, we examined three or four model types with different threshold values for each specimen (Table 1).

Evaluation of 3D morphological data

Because radiolarians achieve a planktonic mode of life by extending pseudopodia to prevent sinking (Takahashi and Honjo, 1983; Febvre-Chevalier and Febvre, 1994; Suzuki and Not, 2015), a lower density is suitable for floating (e.g. Ichinohe *et al.*, 2018, 2019). Given the contributions of both buoyancy and sinking retardation, the weight, volume and surface area are worth calculating.

Dictyocoryne exhibits a triangular shell immediately beneath the cell membrane

(Sugiyama and Anderson, 1997; Suzuki and Aita, 2011). The volume of the shell V_s was calculated from the shell model. In addition, the wrapped model, which mimics living *Dictyocoryne profunda* Ehrenberg with no extension of pseudopodia, was used to estimate the volume of the supposed cell as $V_c = V_w - V_s$, where V_w is the volume of the wrapped model and V_s is the volume of the shell. To calculate the estimated total density of an individual D_t, we adopted a 2.1×10^{-12} g/μm^3 density of opaline silica for the shell D_{op} (Suzuki and Not, 2015) and a 1.03×10^{-12} g/μm^3 density for the cell following the lowest supposed density of *Paramecium* D_c (Hemmersbach *et al.*, 1998), as $D_t = (V_s \times D_{op} + V_c \times D_c) / V_w$. The volume of the wrapped model V_w was also obtained through the calculation of surface area using the function of SC/Tetra (Cradle co. ltd., Japan).

In addition to effortless floating due to a comparatively light shell, one would expect *Dictyocoryne profunda* Ehrenberg to maintain a stable posture in which the equatorial plane of the shell is perpendicular to the direction of sunlight penetration. Typically, the posture of an 'object' with no driving force of locomotion can be explained by its centre of gravity (CG) and buoyancy (CB). In this study, we estimated both the CG of the shell and the CB of the individual without axopodia based on the shell model and the wrapped model using VOXELCON 2014 (Quint Corporation, Japan), respectively.

Results

Effect of the threshold in 3D modelling

The volumes obtained using the shell and wrapped models were compared among three different threshold settings in specimens ID1 to ID3 and four settings in specimen ID4. All of the volumes decreased as the threshold increased (Figure 4), with maximum reductions in shell volume of 40% and the cell volume 72% being observed in specimen ID4 (Table 1).

Figure 5A shows the volumes for all threshold cases relative to length. Both the shell and cell volumes increased monotonically (Figure 5A). Although the absolute values of the volumes varied with respect to the threshold number, each volume was strongly correlated with length (Figure 5A). Based on these results, we hesitated to examine the absolute values of the volumes and their related parameters but performed comparative analyses of the calculated values.

Volumes, densities and surface area of the models

As shown in Figure 5A, the volumes obtained via both the shell and wrapped models (V_s and V_w) increased as length increased, even though the increments differed considerably. For simplicity, all of the relationships are expressed as power functions using a least-square approximation. We obtained $V_s = 1.32 \times L^{2.23}$ ($R^2 = 0.879$) and $V_w = 0.0239 \times L^{3.28}$ ($R^2 = 0.989$), where L is the length of the shell (Figure 5A). Because V_w increased in accordance with the cube law and V_s with the square law, the ratio between shell volume within the supposed cell decreased in larger specimens. The supposed total density D_t of living *Dictyocoryne profunda* Ehrenberg without the extension of pseudopodia was greater than 1.4×10^{-12} g/μm^3 in the case of specimen ID1 (111 μm in length), while the densities of the larger three specimens ID2 to ID4 were greater than 1.1×10^{-12} g/μm^3 in the lowest estimations (Table 1). Thus, all the supposed total densities were greater than that of the seawater (less than 1.03×10^{-12} g/μm^3).

Figure 5B shows calculated weight of the shell W_s (= $V_s \times 2.1 \times 10^{-12}$ g/μm^3), which determined the cell W_c (= $V_c \times 1.03 \times 10^{-12}$ g/μm^3) and their sum as a total weight W (= W_s + W_c). The calculated weights increased as the length increased (Figure 5B). Of these values, the weight of shell W_s with respect to length showed smaller increments, similar to what was found for volume (Figure 5B). In comparison with previous studies of *Dictyocoryne truncata*

(Ehrenberg) and *Spongaster tetras* Ehrenberg (Anderson *et al*., 1989; Sugiyama and Anderson, 1997), the shell weight W_s exhibit a similar trend to that of *Spongaster tetras* (Figure 5B: compare the approximation of W_s with W_{tr}). However, the approximation of W_s is susceptible to error because the shell models of larger individuals with a higher threshold resulted in the underestimation of shell volumes (Figure 4). Using the weights calculated from the shell models with the lowest threshold, we obtained a corrected approximation of $W_{s2} = (9.10 \times 10^{-7}) L^{2.50}$ ($R^2 = 0.984$), which was close to what was observed for *Dictyocoryne truncata* (Ehrenberg) (Figure 5B: compare the approximation of W_{s2} with W_{tr}).

Assuming the weight for the supposed cell without axopodia (= $V_c \times 1.03 \times 10^{-12}$ g/μm^3) was constant regardless of the extension of axopodia, we estimated the ratio of the required cell volume increment relative to the volume of the supposed cell for floating due to neutral buoyancy (Table 1). In the case of specimen ID1 (111 μm in length), neutral buoyancy was associated with 1.7 times the volume of the supposed cell, while for the larger three specimens ID2-4, the corresponding value was 1.2 times (Table 1).

The surface area increased with length, even though the numerical values were considerably smaller than those of the ideal sphere (= πL^2) (Figure 5C). With a power approximation, we obtained a surface area of $S = 0.511L^{2.22}$ ($R^2 = 0.996$), representing a smaller increment in surface area in contrast to an ideal sphere. Unlike the relationship between length and surface area, all of the ratios between surface area and supposed volume (S/V_w) were higher than those estimated for the ideal sphere (Figure 5D). The ratio between surface area and the supposed volume (S/V_w) decreased as the supposed volume increased (Figure 5D).

Centres of gravity (CG) and buoyancy (CB)

The visualised positions of CG and CB are shown in Figures 6 and 7. In the

equatorial plane view, each CG and CB was positioned near the triple arm junction regardless of the specimens (Figures 6, 7). In lateral view, the positions of CG and CB were also close to each other, suggesting no disparity between CG and CB in *Dictyocoryne profunda* Ehrenberg during growth. For specimen ID2 (219 μm in length), the position of CG differed slightly from that of CB according to visual examination. Such differentiation between CG and CB was, however, merely an artefact of remnants of glue at the corner of the shell, which displaced CG towards this corner (see Figure 6E: glue).

Figure 8 shows the calculated values for the distances between the centres of gravity and buoyancy. Except for specimen ID2 with the glue artefact, the distances between CG and CB increased as length increased with normalised values of less than 0.015.

3D morphological features

The smaller shell of specimen ID1 consists of three arms with a comparatively thick skeletal framework, and the stepwise secretion of the patagium and the thin, spongy structure results in a triangular morphology as observed in the larger shells of specimens ID2-4 (Figures 6, 7, 9). As shown in the transmission image of microfocus X-ray CT, secretions from the patagium form a folding layer (Figure 9B, G: white arrowheads). There is no visualised spine in specimen ID1 (Figure 9C), while the other specimens ID2-4 exhibit a spine at the tip of each arm (Figures 6, 7, 9D, E, F). In specimen ID4, the tip of each posterior arm has two spines (Figure 9D, E).

In the equatorial plane view of specimen ID4, the triple junction between the three arms differs from the centre of gravity, because of the smaller angle between the arms beside the patagium, bearing a tubular passway (pylome) for an axoflagellum (Figure 9E). In lateral view, the arms show a gentle sigmoid appearance with a convex shape around the posterior part (Figure 9F). The anterior spine exhibits a tendency to be parallel to an arm, while two

posterior spines obliquely extend in the opposite direction to the axoflagellum (Figure 9F: compare the direction of spine 2 with that of AX). Although the pylome remains unclear in the present 3D models, the difference between the spine angle is recognised in other specimens, such as specimens ID2 and 3 (Figures 6D–F, 7A–C). The pylome continues deep into the triple arm junction nearby but is not perpendicular to the equatorial plane (Figure 9G).

In addition to the pylome, the spines and the shape in lateral view indicate the presence of obverse and reverse faces as we defined in Figure 2. The growth of the three arms appears to follow the extension of the spines, possibly due to the gradual decrease in the growth of the arms along their length as a compromise for thickness.

Discussion

Growth strategy for a planktonic mode of life

To achieve a planktonic mode of life, one plausible explanation is that radiolarians control buoyancy as a function of pseudopodia (see the review work of Suzuki and Not, 2015). Hydrostatically, planktonic behaviour is accomplished by maintaining neutral buoyancy; that is, the net density of the individual is equal to that of the seawater. However, the total density, as estimated in this study, seems too high to maintain neutral buoyancy, unless *Dictyocoryne profunda* Ehrenberg incorporates other biological functions to achieve floating. The extensions of axopodia may play a role in the adjustment of buoyancy to some degree (e.g. Suzuki and Not, 2015), although not to the extent of floating with a positive buoyant force. Given the greater sinking speed of *Dictyocoryne* without the extension of axopodia (Ichinohe *et al*., 2018), it is unlikely to have had a neutral buoyancy for autonomous floating as indicated by the results of Ichinohe *et al*. (2019), even with the increase in size of

air bubbles inside caused by fully extended axopodia (Matsuoka, 2006). Instead, *Dictyocoryne* species could travel with an ambient flow of more than a few μm/s velocity whenever they extend pseudopodia (Ichinohe *et al*., 2019).

Our findings regarding the volumes and weights of the shell and supposed cell imply that the shell of *Dictyocoryne profunda* Ehrenberg presents negative allometry with respect to the growth of the supposed cell, which prevents sinking due to a weight increase. In addition, the surface area of *Dictyocoryne profunda* Ehrenberg is considerably larger than that of a sphere with a similar volume, which enhances sinking retardation due to the viscous resistance. This morphological characteristic contributes to its growth strategy; beginning with the formation of three arms as the structural frame of a triangular shape, the spongy patagium is secreted between the arms and the cell membrane (Matsuoka, 1992). The stepwise secretions of the patagium layer may play a role in constraining the increase in weight. A similar structure to the superficial layers of the patagium is known to exist in *Crassostrea* and *Ostrea* oysters, in which the shells include ample void space (Chinzei, 1995, 2013). In this lightweight structure, the total density of the oyster is lower than that of the surrounding sediments, resulting in adaptation to the soft bottom as if ‘floating’ on the mud (Chinzei, 1995, 2013). The available lines of evidence suggest an analogous growth strategy to retain a lower shell mass.

In addition to the growth strategy of the shell, the function of sinking retardation could be improved with the aid of frictional force from ambient fluids. Typically, a larger surface area of the cell membrane would be beneficial to obtaining frictional force. However, growth would lead to a greater increment of cell volume, which seems to be unreasonable for sinking retardation as demonstrated previously (Ichinohe *et al*., 2018). The flat form is therefore the best form to avoid considerable volume accretion, thereby maintaining a greater viscous resistance for sinking retardation.

Apart from sinking retardation, the surface area of a radiolarian cell may be related to the photosynthetic activity of symbionts. Because radiolarians tend to house symbionts in the ectoplasmic layer (e.g. Anderson, 1976, 1983; Suzuki and Not, 2015), a larger surface area of the cell is advantageous to obtain a greater number of symbionts. The recent technique of epifluorescence microscopic observation revealed that *Dictyocoryne* species exhibit symbionts at the ectoplasmic layer (Takahashi *et al*., 2003). Only case of symbionts in the endoplasm of *Dictyocoryne truncata* (Ehrenberg) was also observed previously (Anderson and Matsuoka, 1992). Although to the questions of why symbionts are in the endoplasm of *Dictyocoryne truncata* (Ehrenberg) remains, a likely possibility is that the symbionts' biological performance depends on nutrients in seawater supplied by the osmotic regulation of the radiolarian as well as the host radiolarian's intracellular medium. Nevertheless, the flat form could provide a large amount of habitable space for symbionts due to the shorter distance from the cell membrane and might enhance the energetic efficiency of photosynthesis (see also Anderson, 1993).

The evidence presented in this study supports the hypothesis that *Dictyocoryne profunda* Ehrenberg achieves a planktonic mode of life with the aid of a lightweight shell and a larger surface area relative to the total volume without autonomously floating due to buoyancy. According to a previous study of radiolarian skeletal growth using a fluorescent compound, only larger individuals with fully developed arms show a phase of skeletal thickening growth (Ogane *et al*., 2010), suggesting quick silicification of the patagium layer. As a result of the growth strategy, *Dictyocoryne profunda* Ehrenberg could convert the large surface area of the flat form into a habitat for photosynthetic symbionts, thereby functionally integrating behaviour, growth and energetic requirements.

A likely scenario of life posture and morphological adaptation

The photosynthetic activity of symbionts may reflect the functional requirements of the life posture (Ichinohe *et al*., 2019). In addition to the adjustment of the life posture by means of pseudopodia (Ichinohe *et al*., 2019), the existence of morphological directions in shell forms may provide postural stability whereby one side of the flat shell could be an obverse or reverse face. For autonomous postural stability, it has been taken for granted that the centres of gravity and buoyancy should be sufficiently distant from each other. In this relationship, *Dictyocoryne* could keep a stable life posture with the side of the centre of gravity oriented downward, as observed for a floating ship. However, there is no gap between their positions, implying that the shell form of *Dictyocoryne profunda* Ehrenberg has no effective function for autonomous postural stability.

In addition to postural stability, it is worthwhile to consider that the centres of gravity and buoyancy are crucial to understanding controllability and manoeuvrability. In aerodynamics, the main and tail wings of an airplane suffer lift forces, altering longitudinal static stability during flight (e.g. von Mises, 1959). The lift forces result in the generation of momentum, acting on the airplane at a point at which the pitching moment coefficient is constant with respect to the lift coefficient, the so-called aerodynamic centre (von Mises, 1959; Brandt *et al*., 2004). To maintain static stability, the aerodynamic centre is generally positioned slightly behind the centre of gravity: the pitching axis of the airplane in lateral view. Less distance between the aerodynamic centre and the centre of gravity causes instability in flight, a functionality that increases agility and manoeuvrability to allow sudden changes in moving direction, as seen in a combat airplane (e.g. Stengel and Berry, 1977).

Returning to *Dictyocoryne profunda* Ehrenberg, we subsequently came to the realisation that the aerodynamic centre is concordant with the centre of buoyancy. The shorter the distance between the centres of gravity and buoyancy, the more likely it is that shell morphology may allow a sudden change in life posture whenever fluid conditions change.

Alternatively, life posture could be managed by means of a modification of gross morphology, as observed in the axopodial extensions (Ichinohe *et al.*, 2019).

One could argue that the flat form of radiolarians leads to unique autecological properties and that the morphological features, as explained herein, have contributed to broad radiation through the photic, shallow marine environment. This scenario is only partly supported by the present study because our results address only the species *Dictyocoryne profunda* Ehrenberg. For example, *Spongaster tetras* Ehrenberg lacks an arm-like tough structure, which makes it lighter in weight than *Dictyocoryne profunda* Ehrenberg. In addition to the differences between growth patterns, the reduced amount of secreted opal results in lighter weight of the individual as shown in Figure 5B. A clue toward understanding the differences between morphological adaptations more clearly lies in the function of the pseudopodia, including the axopodia and axoflagellum. In *Spongaster*, a larger surface area relative to the volume is also advantageous, in that it has many pseudopodia, while the pylome from which the axoflagellum extends places it at the flange of the flat shell (e.g. Sugiyama and Anderson, 1997). In light of the fact that a long pseudopodium, such as the axoflagellum in spumellarians and the axial projection in nassellarians, plays a role in the adjustment of their floating posture (Ichinohe *et al.*, 2018, 2019), an unknown function of pseudopodia may have enabled them to achieve a new level of ecological performance in a planktonic mode of life.

A flat form evolved in the spumellarians more than once during the Phanaerozoic (e.g. Pessagno, 1963, 1971; Nazarov and Ormiston, 1983; Sashida and Tonishi, 1986), suggesting that this form is a typical example of morphological convergence. Unlike previous studies, our approach makes this possibility clear in terms of allometric scaling with morphological adaptation. Further morphological and functional analyses could provide a better explanation of how flat-shaped radiolarians have taken advantage of adaptation under

fluidic seawater conditions.

Acknowledgements

We are grateful to the Sesoko Tropical Biosphere Research Center, University of the Ryukyus for helpful supports with accommodations and field investigations. We thank two anonymous reviewers for their helpful comments and constructive suggestions. This study was financially supported in part by the Sasakawa Scientific Research Grant from The Japan Science Society, by the Research Institute of Marine Invertebrates (Tokyo) 2016KO-2 and by the JSPS KAKENHI Grant Number 25630047 and 25400496.

References

Anderson, O. R., 1976: A cytoplasmic fine-structure study of two spumellarian Radiolaria and their symbionts. *Marine Micropaleontology*, vol. 1, p. 81–89.

Anderson, O. R., 1983: *Radiolaria*, 355 p. Springer Verlag, New York.

Anderson, O. R., Bennett, P. and Bryan, M., 1989: Experimental and observational studies of radiolarian physiological ecology: 1. Growth, abundance and opal productivity of the spongiose radiolarian *Spongaster tetras tetras*. *Marine Micropaleontology*, vol. 14, p. 257–265.

Anderson, O. R., 1993: The trophic role of planktonic Foraminifera and Radiolaria. *Marine Microbial Food Webs*, vol. 7, p. 31–51.

Anderson, O. R. and Matsuoka, A., 1992: Endocytoplasmic microalgae and bacteroids within the central capsule of the radiolarian *Dictyocoryne truncatum*. *Symbiosis*, vol. 12, p. 237–247.

Bramble, D. and Lieberman, D. E., 2004: Endurance running and the evolution of *Homo*. *Nature*, vol. 432, p. 345–352.

Brandt, S. A., Stiles, R. J., Bertin, J. J. and Whitford, R., 2004: *Introduction to Aeronautics: A Design Perspective Second Edition*, 509 p. American Institute of Aeronautics and Astronautics, Inc., Reston.

Chinzei, K., 1995: Adaptive significance of the lightweight shell structure in soft bottom oysters. *Neues Jahrbuch für Geologie und Paläontologie, Abhandlungen*, Band 195, p. 217–227.

Chinzei, K., 2013: Adaptation of oysters to life on soft substrates. *Historical Biology*, vol. 25, p. 223–231.

Febvre-Chevalier, C. and Febvre, J., 1994: Buoyancy and swimming in marine planktonic protists. *In*, Maddock, L., Bone, Q. and Rayner, J. M. V. *eds.*, *Mechanics and Physiology of Animal Swimming*, p. 13–26. Cambridge University Press, Cambridge.

Fujiwara, S., 2018: Fitting unanchored puzzle pieces in the skeleton: appropriate 3D scapular positions for the quadrupedal support in tetrapods. *Journal of Anatomy*, vol. 232, p. 857–869.

Gordon, H. R. and McCluney, W. R., 1975: Estimation of the depth of sunlight penetration in the sea for remote sensing. *Applied Optics*, vol. 14, p. 413–416.

Hemmersbach, R., Voormanns, R., Bromeis, B., Schmidt, N., Rabien, H. and Ivanova, K., 1998: Comparative studies of the graviresponses of *Paramecium* and *Loxodes*. *Advances in Space Research*, vol. 21, p. 1285–1289.

Ichinohe, R., Shiino, Y. and Kurihara, T., 2018: The passive spatial behaviour and feeding model of living nassellarian radiolarians: Morpho-functional insights into radiolarian adaptation. *Marine Micropaleontology*, vol. 140, p. 95–103.

Ichinohe, R., Shiino, Y., Kurihara, T. and Kishimoto, N., 2019: Active floating with buoyancy

of pseudopodia vs passive floating by hydrodynamic drag force: A case study of the flat-shaped spumellarian radiolarian *Dictyocoryne*. *Paleontological Research*, vol. 23.

Ishida, N., Kishimoto, N., Matsuoka, A., Kimoto, K., Kurihara, T. and Yoshino, T., 2015: Three-dimensional imaging of the Jurassic radiolarian *Protunuma* (?) *ochiensis* Matsuoka: an experimental study using high-resolution X-ray micro-computed tomography. *Volumina Jurassica*, vol. 13, p. 77–82.

Ishitani, Y. and Takahashi, K., 2007: The vertical distribution of Radiolaria in the waters surrounding Japan. *Marine Micropaleontology*, vol. 65, p. 113–136.

Kaji, T., Møller, O. S. and Tsukagoshi, A., 2011: A bridge between original and novel states: ontogeny and function of “suction discs” in the Branchiura (Crustacea). *Evolution & Development*, vol. 13, p. 119–126.

Kirk, J. T. O., 1989: The upwelling light stream in natural waters. *Limnology and Oceanography*, vol. 34, p. 1410–1425.

Liu, S., Smith, A. S., Gu, Y., Tan, J., Liu, C. K. and Turk, G., 2015: Computer simulations imply forelimb-dominated underwater flight in plesiosaurs. *PLoS Computational Biology*, vol. 11, e1004605.

Matsuoka, A., 1992: Skeletal growth of a spongiose radiolarian *Dictyocoryne truncatum* in laboratory culture. *Marine Micropaleontology*, vol. 19, p. 287–297.

Matsuoka, A., 1993: Living radiolarians around the Sesoko Island, Okinawa Prefecture. *Fossils (Palaeontological Society of Japan)*, no. 54, p. 1–9. (in Japanese)

Matsuoka, A., 1994: Axoflagellum of discoidal spumellarians (Radioalaria) and axoflagellum pore on their skeletons. *Fossils (Palaeontological Society of Japan)*, no. 56, p. 1–8. (in Japanese)

Matsuoka, A., 2009: Late autumn living radiolarian fauna from sub-tropical surface waters in the East China Sea off Sesoko Island, Okinawa, southwest Japan. *News of Osaka*

Micropaleontologists (NOM), Special Volume, no. 14, p. 11–29.

Matsuoka, A., 2006: Radiolaria–a treasury of form. *In*, Husimi, Y. and Nishigaki, K. *ed*., *Evolution, Information and Form – the Perspective of Biological Knowledge*, p. 142–155. Baifu-kan, Tokyo. (in Japanese).

Matsuoka, A., Yoshino, T., Kishimoto, N., Ishida, N., Kurihara, T., Kimoto, K. and Matsuura, S., 2012: Exact number of pore frames and their configuration in the Mesozoic radiolarian *Pantanellium*: An application of X-ray micro-CT and layered manufacturing technology to micropaleontology. *Marine Micropaleontology*, vol. 88–89, p. 36–40.

Nazarov, B. B. and Ormiston, A., 1983: A new superfamily of stauraxon polycystine Radiolaria from the Late Paleozoic of the Soviet Union and North America. *Senckenbergiana Lethaea*, vol. 64, p. 363–379.

Nomaki, H., LeKieffre, C., Escrig, S., Meibom, A., Yagyu, S., Richardson, E. A., Matsuzaki, T., Murayama, M., Geslin, E. and Bernhard, J. M., 2018: Innovative TEM-coupled approaches to study foraminiferal cells. *Marine Micropaleontology*, vol. 138, p. 90–104.

Nomaki, H., Toyofuku, T., Tsuchiya, M., Matsuzaki, T., Uematsu, K. and Tame, A., 2015: Three-dimensional observation of foraminiferal cytoplasmic morphology and internal structures using uranium–osmium staining and micro-X-ray computed tomography. *Marine Micropaleontology*, vol. 121, p. 32–40.

Ogane, K. and Suzuki, N., 2006: Morphological terms describing discoidal radiolarians. *Revue de Micropaléontologie*, vol. 49, p. 97–104.

Ogane, K., Tuji, A., Suzuki, N., Matsuoka, A., Kurihara, T. and Hori, R. S., 2010: Direct observation of the skeletal growth patterns of polycystine radiolarians using a fluorescent marker. *Marine Micropaleontology*, vol. 77, p. 137–144.

Pessagno, E. A., Jr., 1963: Upper Cretaceous Radiolaria from Puerto Rico. *Micropaleontology*, vol. 9, p. 197–214.

Pessagno, E. A., Jr., 1971: Jurassic and Cretaceous Hagiastridae from the Blake-Bahama Basin (Site 5A, JOIDES Leg I) and the Great Valley Sequence, California Coast Ranges. *Bulletins of American Paleontology*, vol. 60, p. 1–83.

Rayfield, E. J., 2007: Finite element analysis and understanding the biomechanics and evolution of living and fossil organisms. *Annual Review of Earth and Planetary Sciences*, vol. 35, p. 541–576.

Sashida, K. and Tonishi, K., 1986: Upper Permian stauraxon polycystine Radiolaria from Itsukaichi, western part of Tokyo Prefecture. *Science Reports of the Institute of Geoscience, University of Tsukuba, Section B: Geological Sciences*, vol. 7, p. 1–13.

Shiino, Y. and Kuwazuru, O., 2010: Functional adaptation of spiriferide brachiopod morphology. *Journal of Evolutionary Biology*, vol. 23, p. 1547–1557.

Shiino, Y., Kuwazuru, O., Suzuki, Y., Ono, S. and Masuda, C., 2014: Pelagic or benthic? Mode of life of the remopleuridid trilobite *Hypodicranotus striatulus*. *Bulletin of Geosciences*, vol. 89, p. 207–218.

Shiino, Y. and Tokuda, Y., 2016: How does flow recruit epibionts onto brachiopod shells? Insights into reciprocal interactions within the symbiotic framework. *Palaeoworld*, vol. 25, p. 675–683.

Stengel, R. F. and Berry, P. W., 1977: Stability and control of maneuvering high-performance aircraft. *Journal of Aircrait*, vol. 14, p. 787–794.

Sugiyama, K. and Anderson, O. R., 1997: Experimental and observational studies of radiolarian physiological ecology, 6. Effects of silicate-supplemented seawater on the longevity and weight gain of spongiose radiolarians *Spongaster tetras* and *Dictyocoryne truncatum*. *Marine Micropaleontology*, vol. 29, p. 159–172.

Sutton, M. D., Rahman, I. A. and Garwood, R. J., 2014: *Techniques for Virtual Palaeontology*, 208 p. John Wiley & Sons, Ltd, Oxford.

Suzuki, N. and Aita, Y., 2011: Radiolaria: achievements and unresolved issues: taxonomy and cytology. *Plankton & Bentoth Reseach*, vol. 6, p. 69–91.

Suzuki, N. and Not, F., 2015: Biology and Ecology of Radiolaria. *In*, Ohtsuka, S., Suzaki, T., Horiguchi, T., Suzuki, N. and Not, F. *eds*., *Marine Protists. Diversity and Dynamics*, p. 179–222. Springer, Tokyo.

Takahashi, K. and Honjo, S., 1983: Radiolarian skeletons: size, weight, sinking speed, and residence time in tropical pelagic oceans. *Deep-Sea Research. Part A. Oceanographic Research Papers*, vol. 30, p. 543–568.

Takahashi, O., Mayama, S. and Matsuoka, A., 2003: Host-symbiont associations of polycystine Radiolaria: epifluorescence microscopic observation of living Radiolaria. *Marine Micropaleontology*, vol. 49, p. 187–194.

von Mises, R., 1959: *Theory of Flight*, 620 p. Dover Publications Inc., New York.

Yoshino, T., Matsuoka, A., Kurihara, T., Ishida, N., Kishimoto, N., Kimoto, K. and Matsuura, S., 2015: Polyhedron geometry of skeletons of Mesozoic radiolarian *Pantanellium*. *Revue de Micropaléontologie*, vol. 58, p. 51–56.

Yuasa, T., Horiguchi, T., Mayama, S., Matsuoka, A. and Takahashi, O., 2012: Ultrastructural and molecular characterization of cyanobacterial symbionts in *Dictyocoryne profunda* (polycystine radiolaria). *Symbiosis*, vol. 57, p. 51–55.

Zhang, L., Suzuki, N., Nakamura, Y. and Tuji, A., 2018: Modern shallow water radiolarians with photosynthetic microbiota in the western North Pacific. *Marine Micropaleontology*, vol. 139, p. 1–27.

Figure and table captions

Figure 1. Map showing sampling localities. Arrows indicate start and goal points of plankton net towing. TBRC, Tropical Biosphere Research Center, University of the Ryukyus.

Figure 2. Schematic illustration of genus *Dyctyocoryne* in a plane view. **A**, living individual showing axopodia and axoflagellum. **B**, shell and definition of a plane. **C**, terminology of shell morphology. Patagium as shown in B was partially removed to see three arms inside.

Figure 3. Diagram of protocols used in the morphological analyses.

Figure 4. Volumes of the four specimens for different threshold numbers. *L*: length of shell, V_s: volume of shell model, and V_w: volume of wrapped model.

Figure 5. Graphs of numerical values. **A**, volumes of the shell and wrapped models (V_s, V_w). **B**, weight of the four models with respect to length. Dashed lines show power approximation. Total weight W was obtained from the sum of shell weight W_s and cell W_c. W_{s2} indicates power approximation using only the lowest threshold. Note that W_{s2} was close to W_{tr} as estimated in the shell of *Dictyocoryne truncata* (Ehrenberg) (Sugiyama and Anderson, 1997). All of the curves show power approximation. **C**, double-logarithmic graph of surface area of the wrapped model with respect to length. Dashed line showed power approximation in comparison to the sphere shown as a dark grey line. **D**, double-logarithmic graph of ratio of the surface area and volume with respect to volume. Dashed line showed power approximation in comparison with the sphere shown as a dark grey line.

Figure 6. Centres of gravity and buoyancy in plan and lateral views for different threshold numbers. **A**–**C**, specimen ID1. **D**–**F**, specimen ID2. The small dark-grey circle is 10 μm in diameter and shows the centre of gravity (CG), while the large grey circle is 20 μm in diameter and shows the centre of buoyancy (CB).

Figure 7. Centres of gravity and buoyancy in the plan and lateral views for different threshold numbers. **A**–**C**, specimen ID3. **D**–**G**, specimen ID4. The small dark-grey circle is 10 μm in diameter and shows the centre of gravity, while the large grey circle is 20 μm in diameter and shows the centre of buoyancy.

Figure 8. Distances between centres of gravity and buoyancy of all four specimens for different threshold numbers.

Figure 9. Transmission images of microfocus X-ray CT and selected shell models of specimens ID1 and 4 showing morphological features. **A**, transmission image of specimen ID4. Plane view. **B**, lateral view of A. White arrowheads show layers of patagium secretions. **C**, shell model of specimen ID1. **D**, shell model of specimen ID4 for threshold number 40. Plane view. Same with Figure 7D (upper). **E**, shell model of specimen ID4 for threshold number 70. Plane view. Same with Figure 7G (upper). **F**, shell model of specimen ID4 for threshold number 40. Lateral view. Same with Figure 7D (lower). AX, supposed direction of axoflagellum. **G**, longitudinal cross section of D. Black tone shows the section, and the other grey to white area shows the perspective view of the rest. White arrowheads show layers of patagium secretions.

Table 1. Numerical values of morphological analyses.

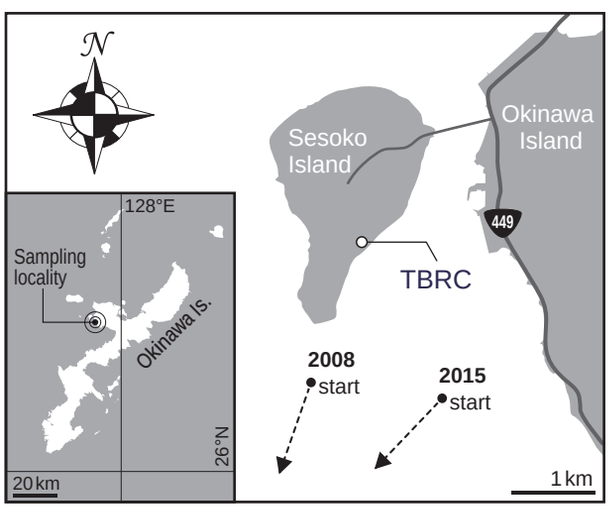

Figure 1 (Shiino et al.)

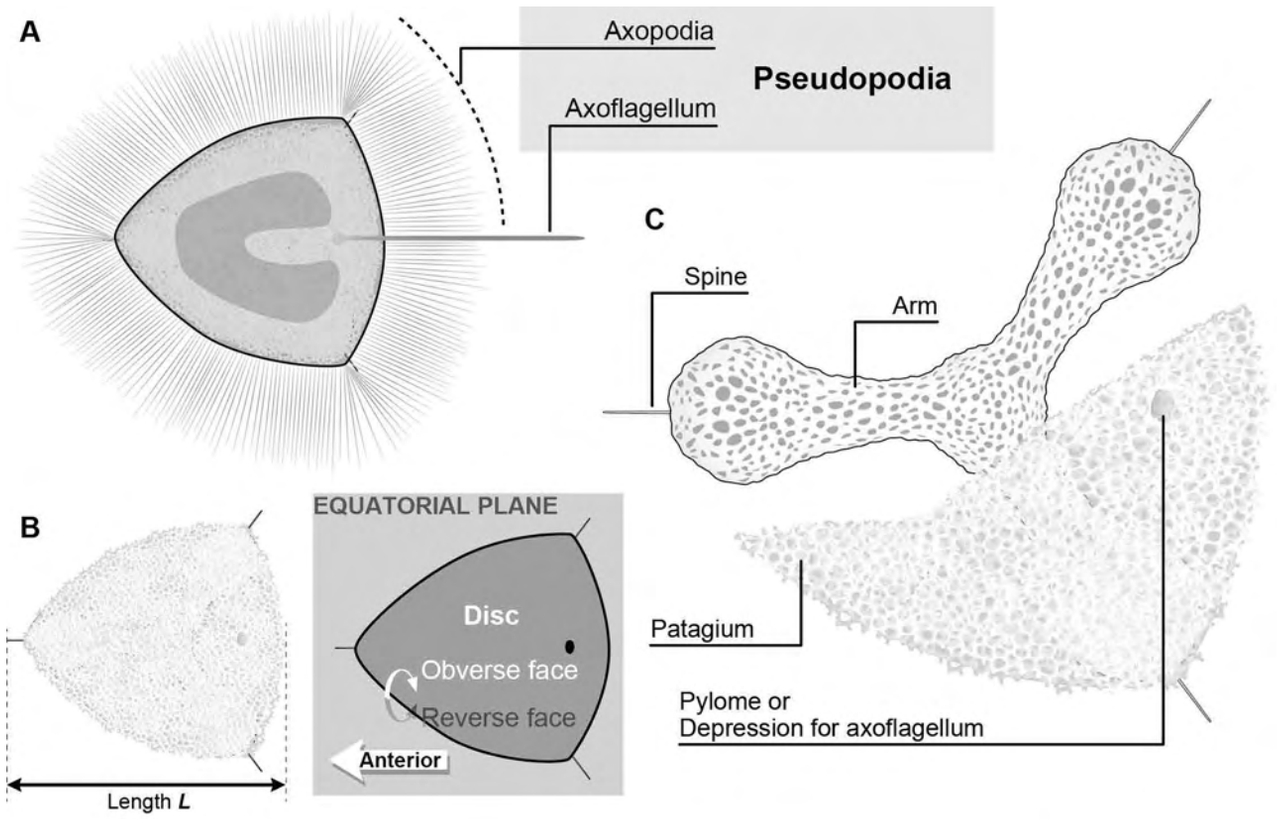

Figure 2 (Shiino et al.)

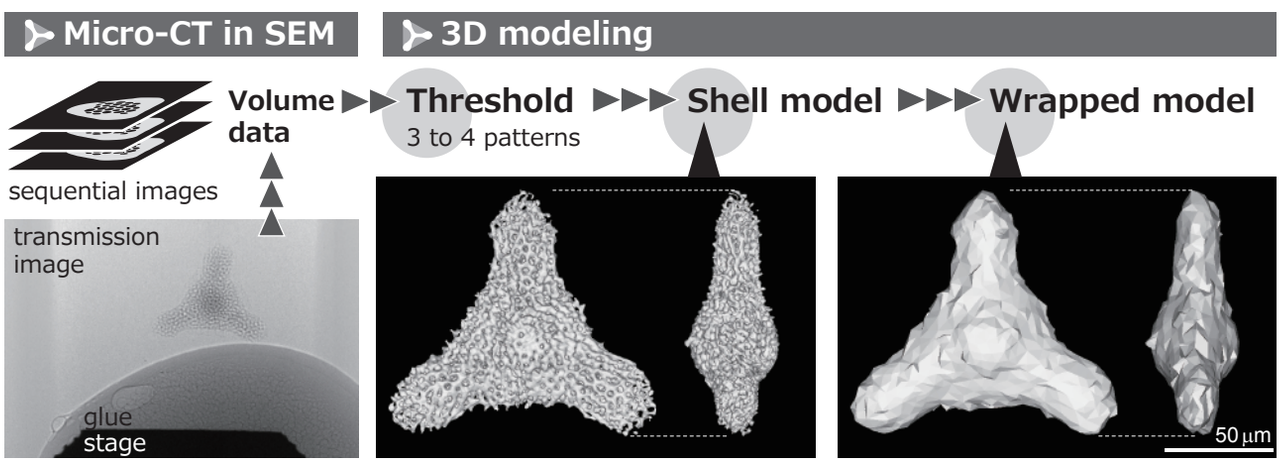

Figure 3 (Shiino et al.)

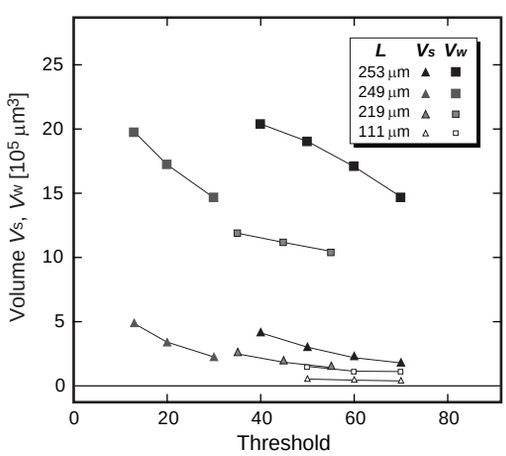

Figure 4 (Shiino et al.)

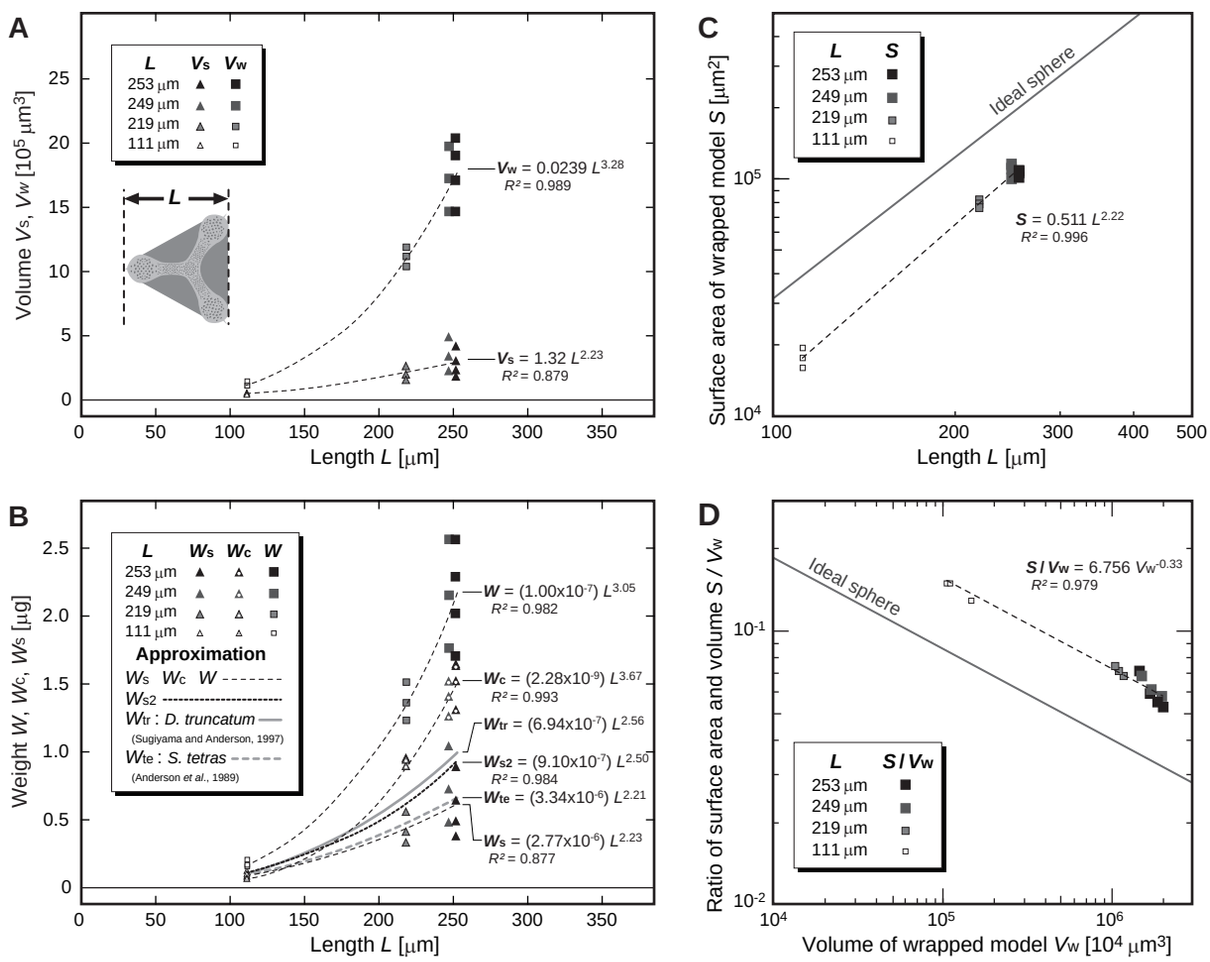

Figure 5 (Shiino et al.)

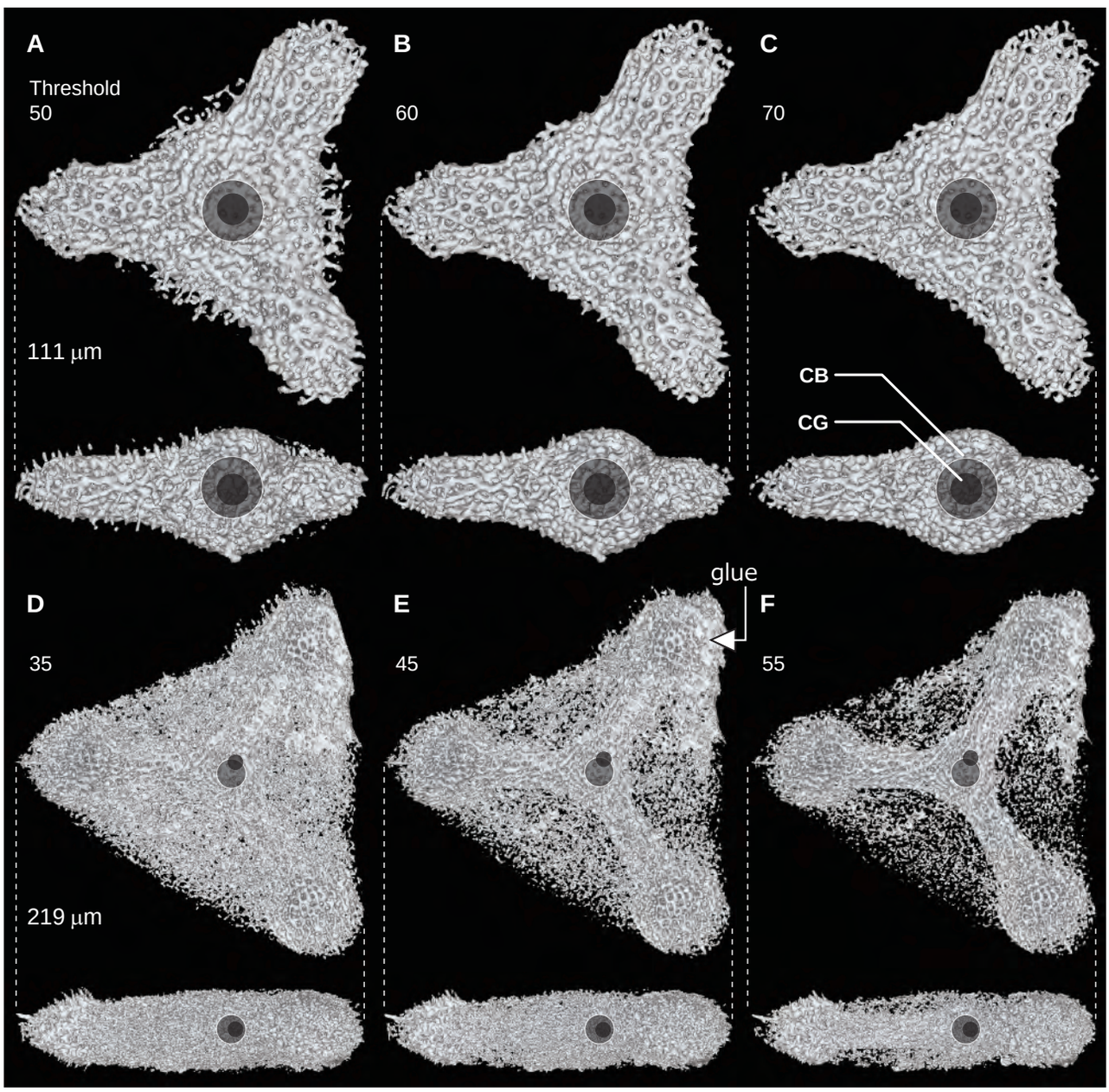

Figure 6 (Shiino et al.)

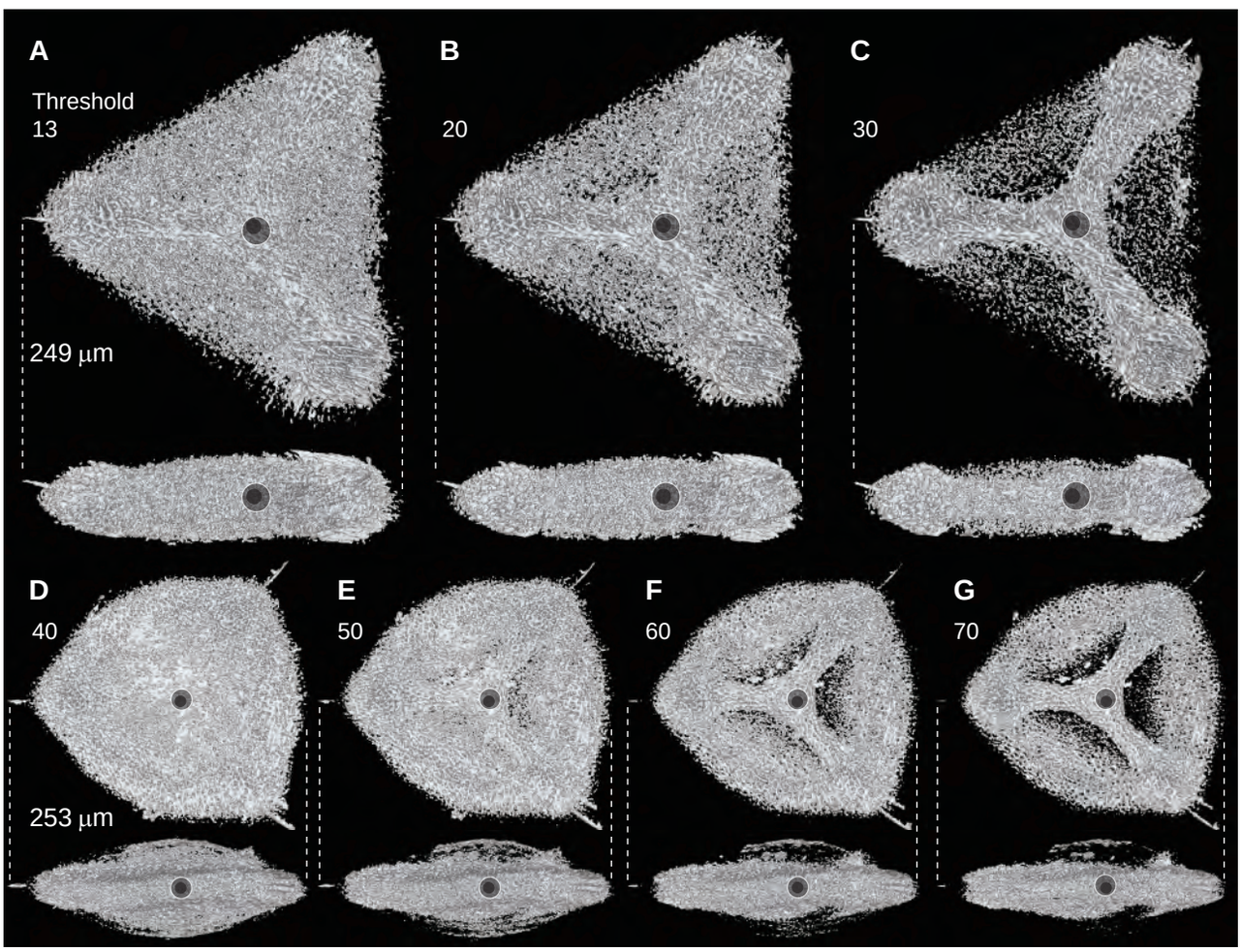

Figure 7 (Shiino et al.)

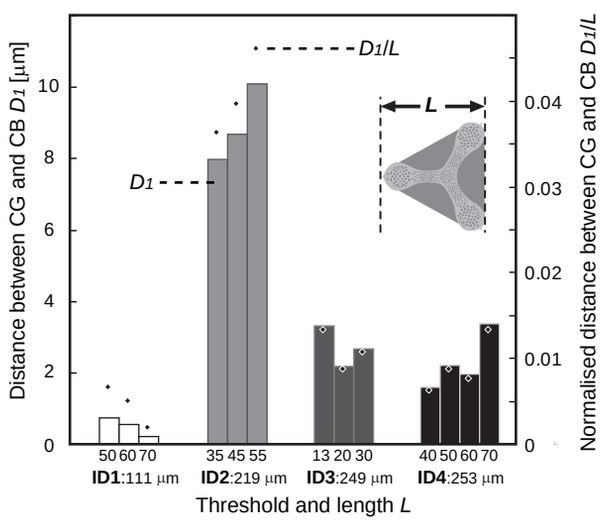

Figure 8 (Shiino et al.)

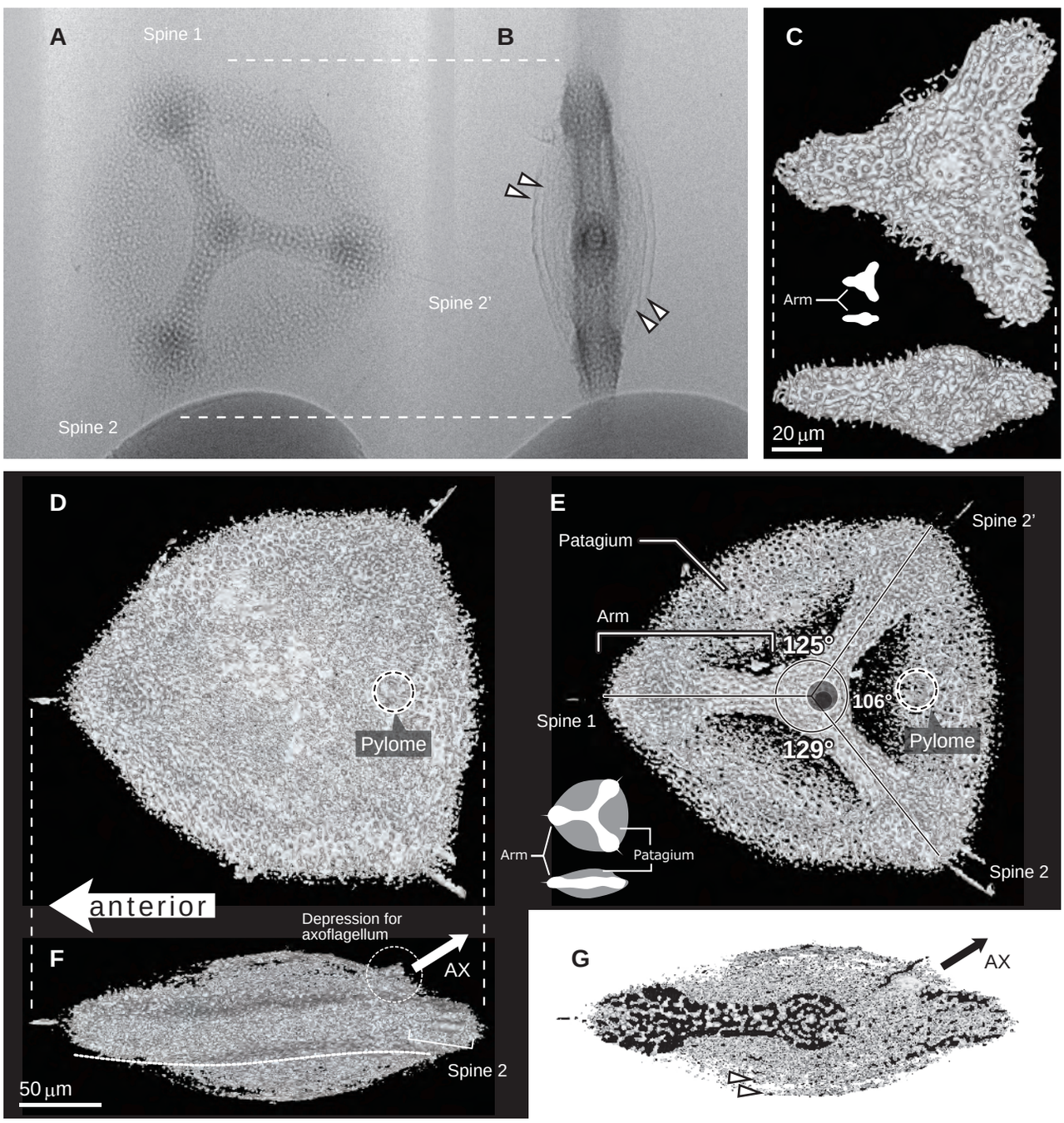

Figure 9 (Shiino et al.)

Table 1. Numerical values of morphological analyses.

Specimen ID of *Dictyocoryne profunda*	Length L [μm]	Threshold	Volume of shell model V_s [μm^3]	Volume of wrapped model V_w [μm^3]	Supposed volume of cell V_c [μm^3]	Calculated weight of shell W_s [μg]	Calculated weight of cell W_c [μg]	Supposed total density D_t [10^{-12} g/μm^3]	Surface area of wrapped model S [μm^2]	Volume ratio of shell and wrapped models V_s/ V_w	Distance between CG and CB D_1 [μm]	Ratio of CG-CB distance and length D_1 / L	Required cell volume increment V_{req} [μm^3]	Ratio of required cell volume increment (V_{req} / V_c)+1
1	111	50	57410	146275	88865	120561	91531	1.450	19050	0.3925	0.735	0.0066	66076	1.7436
		60	47945	110582	62637	100685	64516	1.494	16928	0.4336	0.561	0.0051	55070	1.8792
		70	40169	106032	65863	84355	67839	1.435	16248	0.3788	0.224	0.0020	46268	1.7025
2	219	35	266747	1188199	921452	560169	949096	1.270	81873	0.2245	7.977	0.0364	311950	1.3385
		45	201636	1116120	914484	423436	941919	1.223	79981	0.1807	8.690	0.0397	237921	1.2602
		55	158217	1036103	877886	332256	904223	1.193	78174	0.1527	10.101	0.0461	188245	1.2144
3	249	13	494979	1974550	1479571	1039456	1523958	1.298	115018	0.2507	3.315	0.0133	576622	1.3897
		20	344236	1720839	1376603	722896	1417901	1.244	105865	0.2000	2.174	0.0087	404390	1.2938
		30	230288	1464619	1234331	483605	1271361	1.198	101039	0.1572	2.667	0.0107	273573	1.2216
4	253	40	424447	2033967	1609520	891339	1657806	1.253	107679	0.2087	1.597	0.0063	497765	1.3093
		50	308422	1901178	1592756	647686	1640539	1.204	105165	0.1622	2.215	0.0088	365807	1.2297
		60	234558	1710370	1475812	492572	1520086	1.177	102163	0.1371	1.952	0.0077	280768	1.1902
		70	185187	1462220	1277033	388893	1315344	1.166	105200	0.1266	3.372	0.0133	222756	1.1744